RADAR SIGNAL SPECTRUM DISTORTIONS PRODUCED BY VOLUME AND SURFACE DISTRIBUTED SCATTERERS

Donald E. Barrick

Battelle Memorial Institute
Columbus, Ohio

1968

RADAR SIGNAL SPECTRUM DISTORTIONS PRODUCED BY VOLUME AND SURFACE DISTRIBUTED SCATTERERS

by

Donald E. Barrick

Battelle Memorial Institute
Columbus Laboratories
Columbus, Ohio 43201

prepared for

USNC/URSI Spring Meeting
April 9-12, 1968
National Academy of Sciences
Washington, D. C.

RADAR SIGNAL SPECTRUM DISTORTIONS PRODUCED BY VOLUME AND SURFACE DISTRIBUTED SCATTERERS

by

Donald E. Barrick

Battelle Memorial Institute
Columbus Laboratories
Columbus, Ohio 43201

1. Introduction

When a radar wave strikes a group of volume-distributed scatterers (e.g., raindrops) or surface-distributed scatters (e.g., terrain, sea surface), two things can happen to the incident signal spectrum. First, its center position can be shifted due to relative radial motion between targets and antenna. Secondly, the spectrum shape can be distorted. Since the positions of the scatterers are neither known precisely nor of great concern, the exact shape of the distorted spectrum is not determinable; it is the average effect on the spectrum with which we shall be concerned here. In general, this average spectrum after the interaction is always broadened (though possibly only slightly) from that of the incident signal.

Several mechanisms can produce these spectral distortions. Each of them will be briefly dealt with below. In order to better understand each process, we shall ignore all of the other possible distortion-producing mechanisms while we deal with one at a time. In Section 9 it will be shown how several of these effects can be combined when they act together.

Throughout this article, we shall restrict ourselves to backscatter. The units of the average scattered spectrum, $\sigma(f)$, employed in Sections 5, 6, and 7 below are meters^2 x Hz^{-1} (i.e., backscatter cross section per cycle per second). Then the average backscattering cross section of the distributed scatterers within a single resolution cell is defined as

$$\sigma_B = \int_{-\infty}^{\infty} \sigma(f)df \qquad (1)$$

In sections 2,3, and 4, this spectrum is normalized and given as $P(f) = \sigma(f)/\sigma_B$ because these mechanisms can be treated separately from the scatterers which produce them. In the Appendix, σ_B will be discussed for various scatterer models.

2. Total Signal Length and Its Relationship to Signal Spectrum

The most obvious factor effecting the spectrum of the scattered signal is the spectrum of the incident signal. In the absence of all antenna and target motions, the scattered signal spectrum will be identical to that of the incident signal. In radar systems which attempt to separate moving targets from stationary background or clutter, such as the MTI* system, the total incident signal may consist of a fairly long train of pulses.

One common example illustrating this mechanism is a search radar antenna rotating continuously in azimuth. As the antenna beam rotates past a point target, it is excited by a train of pulses which appear the largest in amplitude as the beam center points directly past the target. The amplitude of this pulse train is modulated by the antenna pattern. Assume that $g(\theta,\varphi)$ is the normalized voltage pattern of the antenna (i.e., $g(0,0) = 1$, where φ here is assumed to be in the azimuth direction and θ is colatitude, perpendicular to it. If the antenna is rotating, then $\varphi = \Omega t$, where Ω is the rotation rate in radians/sec. For backscatter, the received voltage is proportional to g^2, because the same antenna is used for transmitting and receiving. Then the normalized energy density spectrum received from a nonmoving point target at θ_o,φ_o for one sweep of such a rotating antenna consists of a train of spectra spaced f_{PR} (i.e., pulse repetition frequency) apart as shown in Figure 1. Each pulse of the train has the following shape

$$P_n(f) = f_{PR}^2 |F_\tau(nf_{PR})|^2 \cdot \left| \int_{-\infty}^{\infty} [g(\theta_o, \Omega t - \varphi_o)]^2 e^{-i2\pi(f-nf_{PR})t}\, dt \right|^2, \qquad (2)$$

where n is the number of the spectral line ($n = 0$ corresponds to the center carrier frequency position f_o). $F_\tau(f)$ is the Fourier transform of a single normalized pulse of width τ; for a rectangular pulse of unit height, this is $F_\tau(f) = \frac{\sin \pi f \tau}{\pi f}$.

*Moving Target Indication

For instance, assume the antenna pattern is Gaussian, i.e., $[g(\theta,\varphi)]^2 = \exp[-2(\theta^2+\varphi^2)/\Delta^2]$ where Δ is approximately the 3 dB beamwidth of the conical beam. Then one spike in the frequency spectrum, as represented by the square of the integral, or last factor of (2), is $\exp[\pi^2\Delta^2 f^2/\Omega^2]$, where the θ dependence is dropped. Then the total 3 dB width of the spectral line is $\Delta f = \frac{\sqrt{2}\,\Omega}{\pi\Delta}$. For example, the line width for an antenna with a 2° azimuth beamwidth and a rotation rate of 3 rev/sec is $\Delta f \simeq 81$ Hz.

3. Spectral Distortion Due to Relative Motion and Finite Beamwidth

When distributed clutter sources are moving at a velocity, v, through a radar beam, the radial component of this velocity varies slightly across the finite angular width of the beam. This radial velocity variation produces spectral spreading of the incident signal. Assume that the incident signal is monochromatic and all of the particles are moving at the same velocity, v, so that all other sources of spectral distortion can be ignored for the time being.

The analysis here can apply to the case where the antenna itself is in motion with respect to the scatterers, as in an airborne radar. It is also applicable when the scatterers themselves are in motion, as in a rain shower. When the scatterers are volume distributed, as, for instance, raindrops, we will use the geometry of Figure 2a. When the scatterers are surface distributed, as with terrain viewed from an aircraft, we refer to the geometry of Figure 2b. In both cases, v is the velocity of the scatterers moving through the resolution cell with respect to the antenna and α is the angle between v and the direction to the center of the cell.

Assume the same one-way voltage pattern for the antenna, $g(\theta,\varphi)$, as defined in the preceding section. Since the same antenna is used for transmitting and receiving, the power received from a single scatterer within the resolution cell at θ_o, φ_o, is proportional to $|g(\theta_o,\varphi_o)|^4$. The power spectral density received is then obtained by integrating $|g(\theta,\varphi)|^4$ times the reflected power spectrum from a point scatterer at an angle, θ, from boresight. The latter spectrum is an impulse function whose position varies only with θ. Only the integration over θ is of concern here, because this is the angular direction in which the radial

velocity varies and hence the direction producing spectral spreading. Then the spectrum* of the received signal for a monochromatic incident wave of frequency f_o is

$$P(f) = \frac{\sqrt{2}}{\Delta} \frac{1}{\frac{2v}{c} f_o \sin\alpha} \left| g\left(\frac{f - f_o(1 - \frac{2v}{c}\cos\alpha)}{\frac{2v}{c} f_o \sin\alpha}, 0 \right) \right|^4 , \qquad (3)$$

where Δ (in radians) is approximately the 3 dB beamwidth of the one-way power pattern, $|g(\theta,\varphi)|^2$, in the θ direction.** Simply interpreted, this equation shows that the received signal power spectrum has the same shape as the antenna pattern. This result is valid so long as $\alpha \neq 0$. The approximate half-power bandwidth of the received signal may be expressed in terms of the 3 dB antenna beamwidth, Δ: $\Delta f = \frac{\sqrt{2}v}{c} f_o \Delta \sin\alpha$. The Doppler shift of the spectrum center, as seen from (3), is $\frac{2v}{c} f_o \cos\alpha$.

As an example, consider a ground-based S-band (3 GHz) radar looking into a rain shower. Assume it has an elevation beamwidth, Δ, of 3°. Let the look angle above the horizon be 10° (i.e., $\alpha = 80°$). With a moderate rainstorm, the drops fall at a mean velocity of 9 m/s; assume they fall vertically. The Doppler center shift of the received spectrum here is approximately 31 Hz, and the half-power bandwidth for a monochromatic incident signal is about 17.5 Hz. This spectrum spreading caused by raindrops falling through a finite-sized resolution cell is called "shear".

When $\alpha \simeq 0$, the received signal spectrum has approximately the following form:

$$P(f) = \frac{\sqrt{2}}{\Delta} \cdot \frac{1}{\sqrt{\frac{vf_o}{c} \left| f - f_o(1 - \frac{2v}{c}) \right|}} \left| g\left(\sqrt{\frac{c}{vf_o} \left| f - f_o(1 - \frac{2v}{c}) \right|}, 0 \right) \right|^4 . \qquad (4)$$

---

*The spectrum here is normalized so that $\int_{-\infty}^{\infty} P(f)df = 1$.

**For volume-distributed scatterers, the integration over φ is already assumed completed. This is represented in the two-way power pattern beamwidth, $\frac{\Delta}{\sqrt{2}}$; i.e., $\int_{-\infty}^{\infty} |g(\theta,\varphi)|^4 d\varphi \simeq \frac{\Delta}{\sqrt{2}} |g(\theta,0)|^4$ for narrow beam antennas. For surface distributed scatterers, φ is a function of time as the pulse propagates across the ground.

The half-power bandwidth in this case is $\Delta f \simeq \frac{vf_o}{2\sqrt{2}c}\Delta^2$. The above results for $\alpha = 0$ have application to a moving radar, such as that on a homing missile or terrain-avoidance aircraft radar, looking directly ahead. For example, assume that the radar platform is moving at 600 knots and looking straight ahead. At an S-band frequency and for a half-power beamwidth, Δ, of 6°, the spectral spreading due to the finite beamwidth is about 10.6 Hz, while the spectrum center shift is about 6 kHz. This is true for either volume-distributed scatterers, such as rain, or surface-distributed scatterers, such as terrain. One can see that the spectral spreading is not nearly as great when the moving radar is looking ahead as when it is looking off to the side. As a comparison, the same radar, if it were a side-looker, (i.e., $\alpha = 90°$), would have a received spectrum width of about 700 Hz.

4. Spectral Distortion Due to Relative Motion and Finite Resolution Cell Size

A mechanism will be discussed here which produces spectral spreading when a moving radar antenna looks at scatterers distributed throughout the resolution cell. The finite size of the illuminated area is responsible for the spreading. While the mechanisms of the preceding sections are known and have been mentioned elsewhere [1], this mechanism, we believe, has not been recognized previously as a contributor to spectral spreading. The effect is illustrated in Figure 3. The component of velocity in a direction containing the plane of incidence is v. The range resolution cell depth is $\frac{c\tau}{2}$ for volume-scatterers, and $\frac{c\tau}{2\cos\beta}$ if the radar is looking at the ground at a depression angle β. The velocity, v, for the latter case is assumed to be that component parallel to the ground. Assume that the return at radar position #1 for elapsed time, t_a, comes from the solid resolution cell. Then at the time of the next pulse transmission, the radar platform has moved, and at elapse time t_a, the returning pulse comes from the dashed resolution cell. These two resolution cells do not contain identically the same scatterer targets, but a portion of them are shared by the two. As the velocity increases, there is less overlap, but as the resolution cell length increases, the overlap becomes greater. The signal returns from the non-overlapping areas are uncorrelated from pulse to pulse, because they contain different scattering centers at different positions.

If we compute the correlation coefficient for the overlapping areas as a function of elapsed time, T, we find it is

$$R(T) = \begin{cases} 1 - \left|\frac{vT}{L}\right| & \text{for } \left|\frac{vT}{L}\right| < 1 \\ 0 & \text{for } \left|\frac{vT}{L}\right| > 1 \end{cases}$$

, where L is the length of the resolution cell in the direction of motion (i.e., it is $\frac{c\tau}{2}$ and $\frac{c\tau}{2\cos\beta}$ for the cases mentioned above).

The Fourier transform of this correlation function is then the normalized density spectrum for the received signal when the incident carrier is monochromatic. It is

$$P(f) = \frac{\sin^2\left(\frac{\pi L}{v} f\right)}{\pi^2 \frac{L}{v} f^2} \quad . \tag{5}$$

The approximate half-power bandwidth of this spectrum is $\Delta f \approx \frac{v}{L}$.

As an example, consider an aircraft with a narrow pulse ($\tau = 0.1\ \mu s$) flying at 600 knots and looking straight ahead. If the depression angle, β, is small, the length of the resolution cell, L, is $\frac{c\tau}{2}$. Then the half power bandwidth of the received spectrum is 20 Hz.

The mechanism here is definitely different from that of the preceding section, which depended upon the fact that, due to finite beamwidth, the wave phasefront is not planar across the resolution cell but spherical. In other words, the rays propagating to different parts of the resolution cell are not parallel, with the angle between them and the velocity vector varying. The mechanism of this section produces spectral spreading even if the rays are parallel and the phase front is planar. A comparison of the two processes results in some interesting contrasts. The preceding section showed that decreasing the size of the resolution cell by making the beamwidth smaller decreases the spectral spreading; this section shows that decreasing the length of the resolution cell can increase the spectral spreading, because of the different mechanism involved. From (5), one can see that as either the velocity approaches zero or as the resolution cell length approaches infinity, the scatterer spectrum approaches the impulse function. This is expected since the incident spectrum is an impulse function, and when there is no apparent motion, the scattered spectrum should also be an impulse.

5. Spectral Distortion Due to Volume Scatterer Velocity Differences

One sometimes encounters volume-distributed scatterers whose velocities are not all identical. Such is the case for raindrops, whose fall velocities are observed to vary with drop size.* Figure 4 illustrates the geometry for a packet of particles moving in the vertical direction, while the radar views it from angle, α, with respect to the vertical. The individual particles are assumed to be all moving in the same direction, but have different speeds, i.e., v_1, v_2, v_i, ... We can now define and assign p(v) as the probability density function for the velocity of a given particle.

A monochromatic signal illuminates the particles, and hence the incident spectrum is proportional to the unit impulse function, $\delta(f-f_o)$. Then it may be shown in a straightforward manner that the signal reflected from all of the particles has a power density spectrum proportional to the particle velocity probability density. Expressed as the radar cross section per unit frequency, $\sigma(f)$, this is

$$\sigma(f) = \frac{c}{2f_o\cos\alpha}\, p\left(\frac{f-f_o}{(2f_o\cos\alpha/c)}\right)\sigma_B \quad , \tag{6}$$

where σ_B is the radar cross section of all of the particles within the resolution cell. If the standard deviation (or square root of the variance) of the particle velocity is v_{sd}, then the approximate half-power bandwidth, Δf, of the scattered signal spectrum is given as $\Delta f = \frac{4v_{sd}}{c} f_o \cos\alpha$.

Let us look at an example. Mean drop velocities in a rainfall are about 4-6 m/s for light rains to 9 m/s for heavy rains [2]. The standard deviation of drop velocities about the mean is approximately 1 m/s. For an S-band (3 GHz) radar in a heavy rainfall and at an elevation angle of 10° (i.e., α = 80°), the

---

*Neglected here are any rotational velocities of individual particles. For instance, a rotating chaff particle will modulate the incident signal. For nearly spherical raindrops, this effect is not applicable.

center frequency of the return will be shifted by about 31 Hz. The scattered spectral width for an incident monochromatic wave will be 7 Hz. It has been observed, however, that a significant number of smaller sized raindrops fall very slowly; this results in a gradual tapering off of p(v) below the mean velocity of 9 m/s, but a much more abrupt cutoff above the mean. Hence even though the predicted half-power width is 7 Hz, we can expect to see scattered signal energy in a band as great as 30-40 Hz, since the spectrum does not fall off rapidly below the lower 3 dB point. The spreading also increases with elevation angle; if the radar is looking vertically ($\alpha = 0°$), the spread can be as great as 200 Hz at S-band.

Another example illustrating this mechanism is foliage motion due to wind. A surface search radar, for instance, looking over a wooded area will receive a return from the trees and foliage whose spectrum is spread due to leaf and branch motion. Nathanson [3] has found from examination of experimental data that the standard deviation of foliage velocity for wooded terrain is about 0.03 m/s for a 0-10 knot wind, about 0.1 m/s for a 15 knot wind, and about 0.3 m/s for a 20 knot wind. An S-band (3 GHz) surface search radar looking along the horizontal in the wind direction ($\alpha = 0$) will suffer a spectral spread from the foliage return of about 4 Hz for 20 knot wind.

6. Spectral Distortion from Sea Surface Due to Surface Movement: Slightly Rough Surface

The sea surface represents a case of surface-distributed scatterers which are in motion. One would naturally expect to see a distortion of the received radar spectrum due to a random modulation of the incident wave by the sea. This section will be concerned with the roughness whose scale falls into the category "slightly rough"; by this we mean that $k_o h \cos\theta_i < 1$, where $k_o = \frac{2\pi}{\lambda}$ is the free space wavenumber, h is the rms height of the ocean waves, and θ_i is the incidence angle measured from vertical (i.e., the complement of the grazing angle). At HF frequencies, all of the ocean waves in general satisfy this criterion, while at microwave frequencies, only the capillary waves may fall in this category.

It is shown in Reference 4 that surfaces having slightly rough scales must be analyzed by a perturbation technique. Such an analysis, valid in the low-frequency limit, shows a difference in return for vertical and horizontal polarization states which agrees with experimental observations. The analysis there, valid for a two-dimensionally rough surface height variable $z = \zeta(x, y)$, can be readily extended to include a third quantity, time, i.e., $z = \zeta(x, y, t)$. The analysis proceeds as before, but with three instead of two variables. Details of the derivation are omitted here for lack of space. The radar (backscatter) cross section per Hz bandwidth for a surface area, A, included within the resolution cell is

$$\sigma(f) = 4\pi^2 k_o^4 A \cos^4\theta_i |\alpha(\theta_i)|^2 W_1[-2k_o \sin\theta_i,\ 0,\ 2\pi(f-f_o)] \ . \qquad (7)$$

The quantity $W_1(p,q,\omega)$ is the spatial and temporal height spectral density of the slightly rough ocean surface scale. It is defined in terms of the surface height correlation function, $h^2 R_1(X, Y, T) = \langle \zeta(x,y,t)\zeta(x+X, y+Y, t+T) \rangle$ as follows

$$W_1(p,q,\omega) = \frac{h^2}{\pi^3} \int_{-\infty}^{\infty} \int_{-\infty}^{\infty} \int_{-\infty}^{\infty} R_1(X, Y, T) e^{-ipX - iqY - i\omega T} dX dY dT. \qquad (8)$$

Here, $\zeta(x,y,t)$ is taken to be the surface height above the mean level, and hence its average value is zero. Also, $\alpha(\theta_i)$ in (7) is proportional to the polarization matrix elements; it varies with incidence angle and surface constitutive parameters, but is not a function of the roughness. It will be given in the Appendix for the vertical and horizontal polarization states.

Equation (7) shows that only the ocean wave spatial frequency $p = 2k_o \sin\theta_i$ produces backscatter. Stated another way, the entire backscattered component at radar wavelength λ is produced by those ocean waves of length $L = \lambda/2\sin\theta_i$. This result has been mentioned many times in the literature.

The spatial spectrum of the sea surface, $W_1(p, q)$, has been measured and the ~~Neyman~~ Neumann-Pierson model [5] seems to explain its dependence upon wind. No

one has yet measured the full spatial and temporal spectrum of the sea, and no one has proposed a reasonable theory or model for it. First order ocean wave theory shows that the temporal period of the sea has a deterministic relationship with respect to the spatial wavelength for a given wave. In other words, an ocean wave of given length has a fixed period, determined by the forces of gravity and fluid mechanics at the air-water interface. This first-order relationship between the ocean surface spatial wavenumbers p, q, and the temporal wavenumber, ω ($\omega = 2\pi f$), is $\sqrt{p^2+q^2} = \frac{\omega^2}{g}$, where g is the acceleration of gravity [5]. If one employs this first-order approximation, Equation (7) shows the received spectrum to be two impulse functions at frequencies $f = f_o \pm \frac{g^{1/2}}{2\pi}\sqrt{2k_o \sin\theta_i}$. Radar measurements at HF have shown that the position of the spectrum is predicted by the above relationship, but the spectrum is not an impulse function.[6] It has a finite width which can be several tenths of a Hz at $f_o \simeq 13$ MHz. This suggests that one must go beyond the first-order theory to obtain a meaningful estimate of the spatial and temporal sea spectrum contained in (7).

7. Spectral Distortion From the Sea Surface Due to Surface Movement: Very Rough Surface

At microwave frequencies, the largest scale ocean waves are greater in height than the radar wavelength. This large scale, satisfying the relationship $k_o h \cos\theta_i > 1$, is called "very rough", and is analyzed by physical or geometrical optics. The result, valid in the high-frequency limit, shows that all scatter comes from portions of the surface oriented normal to the radar line of sight;[7] these are called specular points and are familiar at optical frequencies as the dancing glitter of the sun on the surface. Since these specular points are in motion, they produce random shifts in the frequency of the incident wave. The analysis of a moving surface has been treated extensively in [8].

As in the above section, one can determine the scattered power from such a surface by merely extending previous analyses for a random surface, $\zeta(x,y)$, to include the time variable also, i.e., $\zeta(x,y,t)$. Using the physical optics formulation, one can arrive at the following result for the radar cross section per Hz bandwidth.

$$\sigma(f) = \frac{Ac}{4f_o} \sec^5\theta_i |R(0)|^2 P\left(\tan\theta_i,\ 0,\ \frac{f-f_o}{(2f_o\cos\theta_i)/c}\right) \qquad (9)$$

where $P(\zeta_x, \zeta_y, \zeta_t)$ is the joint probability density function for the surface slopes ζ_x and ζ_y in the x- and y-directions* and for the vertical surface velocity, ζ_t (i.e., $\zeta_t = \partial\zeta/\partial t$). Also, R(0) is the Fresnel reflection coefficient for the sea for normal incidence, and A is the surface area within the resolution cell. Normally, ζ_x, ζ_y, and ζ_t are correlated to a considerable extent so that it is not possible to separate $P(\zeta_x, \zeta_y, \zeta_t)$ into the product of separate density functions.

Notice the similarity between (9) for sea surface motion and (7) for volume scatterer motion. Even though the two theories were derived from different initial formulations, the similarity between results indicates that the mechanism producing spectral spreading is the same: it is the motion of discrete scattering centers separated on the average by many wavelengths. In the former case, the discrete scattering centers were individual particles, such as raindrops, whereas in the latter case, they are the moving specular points on the surface.

As pointed out previously, the three derivatives of the surface are normally correlated. For the sake of obtaining an estimate of the sea spectral spreading produced by the large scale roughness, let us assume they are uncorrelated. Further, let us assume that the surface is Gaussian. Then it is easy to show that the variance of the vertical ocean wave velocity is $v_{sd}^2 = \langle\zeta_t^2\rangle = \frac{2h^2}{T^2}$, where h^2 is the mean-square surface height and T is roughly the time period of the large scale ocean waves. Measurements have shown that 1 m/s is typical of v_{sd} for the sea surface. The half-power spectral width of the received power is $\Delta f \simeq \frac{4v_{sd}}{c} f_o\cos\theta_i$. For an S-band radar (3GHz) and at a depression angle of 10° (i.e., $\theta_i = 80°$), this half-power bandwidth is $\Delta f \simeq 8$ Hz, using $v_{sd} \simeq 1$ m/s.

8. Spectral Distortion From the Sea Surface Due to Surface Movement: Composite Surface

At microwave frequencies, the sea surface definitely has a large-scale component compared to radar wavelength. However, it also has a small-scale component (i.e., the capillary waves) which ride on top of the larger structure and fall into the slightly rough category. Hence, the scattering mechanisms of both of the preceding sections appear to be operating simultaneously.

(*The plane of incidence is assumed for convenience to be the x-z plane)

It is shown in [4] and discussed in [9] that to a first order, one can represent the scattered power from such a composite surface as the sum of the powers from the very rough and slightly rough scale components. One adds the powers because these two roughness scales are usually independent of each other (being produced by different mechanisms) and hence they, the scattered fields, superpose incoherently.

The same reasoning can be applied to the spectrum from such a surface. One therefore adds $\sigma(f)$ of (7) to that of (9) to obtain the backscattered spectrum of a composite surface for an incident monochromatic wave. One has two actual surfaces to analyze in this case, ζ_L and ζ_S, where ζ_L includes all large-scale surface height components which satisfy $k_o\zeta_L\cos\theta_i > 1$ and ζ_S includes the small-scale components failing this inequality. The combination of the two mechanisms simultaneously results in a complicated model which is a function of several parameters. Qualitatively, one can see that as one approaches grazing ($\theta_i \to \pi/2$), the slightly rough theory becomes more important because more of the ocean roughness satisfies the inequality $k_o\zeta\cos\theta_i < 1$.

What does experimental evidence show about the scattered signal spectrum in the microwave frequency region? Not enough data is available to obtain a complete and accurate picture as a function of polarization, frequency, sea state, incidence angle, etc. Some of the data seems to confirm the validity over a limited range of the expression $\Delta f = \frac{2\Delta v}{c} f_o$ for the half-power bandwidth, where Δv is a sea-surface velocity spread. From [3] and [10], Δv varies approximately linearly from about 0.7 m/s for Sea State #1 (wind speed 5 knots), being about 1.8 m/s for Sea State #3 (wind speed 13 knots), to about 2.7 m/s for Sea State #5 (wind speed 22 knots). Measurements show that Δv may be somewhat larger than these values for horizontal polarization and somewhat lower for vertical polarization (by as much as 20-30%). For example, at S-band (3 GHz), one can expect spectral spreading by as much as 55 Hz for Sea State #5 from this measured data.

9. Combination of Several Spectral Distorting Effects

In Sections 2 through 8, we have considered various known physical mechanisms which distort the spectrum of an incident signal after scattering.

To physically understand them, we treated each mechanism separately ignoring all of the other possibilities. In reality, several of the processes are usually acting simultaneously. For instance, one may have the spectrum-distorting effect of finite beamwidth discussed in Section 3, as well as sea surface motion. How then does one combine these various effects to obtain the total spectrum of the received signal?

One can show theoretically that the resultant signal spectrum, $\sigma_R(f)$, expressed in terms of average radar cross section per Hz bandwidth, is obtained by convolving the various spectra together. For instance, let $P_i(f)$ be the normalized spectrum of the incident signal. Assume that the radar platform is moving, and looking down across the sea surface. Then the effect of finite beamwidth given in (3) must be included: call it $P_1(f)$. Also, the motion of the sea surface distorts the spectrum according to the mechanisms in Sections 6-8; this is represented as $\sigma(f)$. In addition, the effect mentioned in Section 4 may be important; let us assume it is not significant here. Then the total received spectrum is given by

$$\sigma_R(f) = \int_{-\infty}^{\infty} \int_{-\infty}^{\infty} P_i(\eta) P_1(\xi-\eta)\, \sigma(f-\xi)\, d\eta\, d\xi \quad . \tag{10}$$

While the above convolution technique is exact, it is unfortunately not very handy when the various spectra are only estimates to start with. Nor is it convenient when a quick answer is needed. A simpler "rule of thumb" is available. It is obtained from the above equations when one assumes that at least two of the three processes are random and that all three are mutually independent. The total 3 dB bandwidth, Δf_R, may be found from the bandwidth of the incident signal, Δf_i, the bandwidth, Δf_1, of $P_1(f)$, and the bandwidth, Δf_s, of $\sigma(f)$ for the sea surface:

$$\Delta f_R^2 = \Delta f_i^2 + \Delta f_1^2 + \Delta f_s^2 \quad . \tag{11}$$

10. Summary

In this paper we have attempted to mention and briefly discuss all of the known mechanisms which produce spectral distortions on an incident signal after

scatter from distributed sources. Some of these mechanisms have been mentioned previously [1], but we have attempted here to relate the spectral distortions more precisely to the antenna and signal properties. The mechanism mentioned in Section 4 has not been previously recognized as a contributor to scattered spectrum distortions. The movement of the slightly rough sea surface scale (Section 6) produces a spectral distortion somewhat different from that induced by usual scatterer motions of Sections 5 and 7. The signal spectrum for the slight scale movement is directly proportional to the temporal spectrum for the surface height itself.

In most radar applications the volume-and surface-distributed scatterers represent unwanted background, or clutter, as in the case of rain and terrain. However, there are situations, such as in satellite, air surveillance, and ground-mapping, as well as with weather radars, where one is primarily interested in observing these targets. In either case, the results presented here, along with the physical interpretation provided, should aid in analysis of the received signal.

Appendix. Scattering Cross Section for Distributed Scatterers

(a) Volume-Distributed Scatterers

In Equation (6), we expressed the radar (backscatter) cross section of all of the volume-distributed scatterers within a radar resolution cell as σ_B. Here we wish to examine this quantity further, break it down, and provide a meaningful physical explanation of the scatter mechanism.

It is shown in [10] that one can express σ_B in terms of the radar cross section per unit volume times the volume of space inside the resolution cell, i.e., $\sigma_B = \sigma^c V$. The depth of the resolution cell is $\frac{c\tau}{2}$ where τ is the signal pulse length. The cell is elliptical in shape looking along the antenna boresight, with Δ and ϵ being the half-power beamwidths of the one-way antenna directivity pattern, $|g(\theta,\varphi)|^2$. Since the same antenna is assumed to be used twice for the backscatter situation, the two-way half-power beamwidths for narrow-beam patterns are approximately $\frac{\Delta}{\sqrt{2}}$ and $\frac{\epsilon}{\sqrt{2}}$ (if the beam is conical, $\Delta = \epsilon$). Then the volume inside this cell is given as

$$V = \left[\pi R^2 \cdot \frac{1}{4} \frac{\Delta}{\sqrt{2}} \frac{\epsilon}{\sqrt{2}}\right] = \frac{\pi R^2 c\tau \Delta\epsilon}{16} \quad , \tag{12}$$

where R is the range to the cell from the antenna.

The quantity σ^c is discussed in detail in [10]. A simple and meaningful model is presented there; each particle, while its position is entirely random, is assigned an average individual radar cross section, $\langle\sigma\rangle$. Then it is shown that, due to the random position assumption, one can add the average scattered power from each particle incoherently to obtain the following result for the average total radar cross section per unit volume:

$$\sigma^c = \rho \langle\sigma\rangle \quad , \tag{13}$$

where ρ is the scatterer density, or average number of particles per unit volume.

For raindrops, $\langle\sigma\rangle$ is the backscatter cross section of a small water sphere. Since this raindrop size is small compared to wavelength in the microwave region, one can use the low-frequency approximation for a dielectric sphere.

Experimentally, values of drop density, ρ, of the order of $100/m^3$ for rain have been measured. Also, values of σ^c have been measured for a moderate rainfall varying from -83 dB at S-band, -62 dB at X-band, up to -39 dB at K_a-band (expressed as dB m^{-1}).

(b) Surface Scatter: Slightly Rough Surface

Rough surfaces falling in the slightly rough category have been treated elsewhere [4], [9], [10], [11]. Here we shall briefly mention the result obtained for this model. First, we express the average radar cross section for the surface within a resolution cell as $\sigma_B = \sigma^\circ A$, where A is the surface area subtended by the resolution cell and σ° is the average backscatter cross section per unit area. For the radar configuration shown in Figure 2b, the area A is given by

$$A = \left[\frac{R\Delta}{\sqrt{2}}\right]\left[\frac{c\tau}{2\cos\beta}\right] = \frac{Rc\tau\Delta}{2\sqrt{2}\sin\theta_i} \quad , \tag{14}$$

where β is the grazing angle and $\theta_i = \pi/2-\beta$. All other symbols have been defined previously.

Actually, σ° can be obtained from (7) by performing the integration indicated in (1), or it can be derived separately, as done in [4]. In either case, it becomes

$$\sigma^\circ = 4\pi k_o^4 \cos^4\theta_i \, |\alpha(\theta_i)|^2 W_1[-2k_o\sin\theta_i, \; 0], \tag{15}$$

where $W_1(p,q)$, the spatial spectrum of the surface height, is defined from the two-dimensional surface height correlation function, $h^2R_1(X, Y)$ as in (8):

$$W_1(p,q) = \frac{h^2}{\pi^2}\int_{-\infty}^{\infty}\int_{-\infty}^{\infty} R_1(X, Y)\, e^{-ipX-iqY}\, dXdY \quad . \tag{16}$$

Also, $\alpha(\theta_i)$ is derived in [4] for the vertical and horizontal polarization states. For a homogeneous surface having relative constitutive parameters ϵ_r, μ_r, they are:

$$\alpha_{hh}(\theta_i) = \frac{(\mu_r-1)\left[(\mu_r-1)\sin^2\theta_i + \epsilon_r\mu_r\right] - \mu_r^2(\epsilon_r-1)}{\left[\mu_r\cos\theta_i + \sqrt{\epsilon_r\mu_r-\sin^2\theta_i}\,\right]^2}$$

$$\alpha_{vv}(\theta_i) = \frac{(\epsilon_r - 1)\left[(\epsilon_r - 1)\sin^2\theta_i + \epsilon_r\mu_r\right] - \epsilon_r^2(\mu_r - 1)}{\left[\epsilon_r\cos\theta_i + \sqrt{\epsilon_r\mu_r - \sin^2\theta_i}\,\right]^2},$$

$$\alpha_{hv}(\theta_i) = \alpha_{vh}(\theta_i) = 0. \tag{17}$$

For a perfectly conducting surface, one permits $\epsilon_r \to \infty$ in the above equations to obtain

$$\alpha_{hh}(\theta_i) = 1, \qquad \alpha_{vv}(\theta_i) = \frac{1 + \sin^2\theta_i}{\cos^2\theta_i} \tag{18}$$

The above results are valid only to the first order in $(k_o\zeta\cos\theta_i)^2$, ζ_x^2, and ζ_y^2. They indicate no depolarization for these states. Retention of higher order terms does include depolarization, although the results are considerably more complex [12].

(c) Surface Scatter: Very Rough Surface

If the surface roughness falls in the "very rough" category, results for σ° analogous to those of the last section can be obtained. These are found either by integrating (9) as shown in (1), or by a separate derivation [4]. The result is

$$\sigma^\circ = \pi\sec^4\theta_i\,|R(0)|^2 P(\tan\theta_i, 0), \tag{19}$$

where $P(\zeta_x, \zeta_y)$ is the joint probability density function of the surface slopes ζ_x, ζ_y in the x- and y-directions. All of the other quantities have been defined before.

Further details and comparison with measured data σ° may be found in [10] and [11].

REFERENCES

1. Steinberg, B. D., "Target, Clutter, and Noise Spectra", pp. 473-484, Modern Radar. Analysis, Evaluation, and System Design, ed. by R. S. Berkowitz. New York: John Wiley & Sons, (1965).

2. Medhurst, R. G., "Rainfall Attenuation of Centimeter Waves: Comparison of Theory and Measurement", IEEE Trans. Ant. Prop., AP-13, pp. 550-564, (1965).

3. Watters, E. C., and F. J. Nathanson, "Radar and Clutter", Short Course Notes, University of Alabama in Huntsville, November, 1967; also, Radar Signal Processing, by F. J. Nathanson, McGraw-Hill Book Co., to be published.

4. Barrick, D. E., and W. H. Peake, "Scattering from Surfaces with Different Roughness Scales: Analysis and Interpretation", Battelle Memorial Institute, Columbus Laboratories, Columbus, Ohio, Rept. BAT-197A-10-3, November 1, 1967, AD 662 751; also published under separate cover by The Electroscience Laboratory, The Ohio State University, as Rept. 1388-26.

5. Kinsman, B., Wind Waves. Englewood Cliffs, N. J.: Prentice-Hall, Inc., pp. 117-133, (1965).

6. Crombie, D. D., "Doppler Spectrum of Sea Echo at 13.56 Mc/s", Nature, 175, pp. 681-682, (1955).

7. Barrick, D. E., "Rough Surface Scattering Based on the Specular Point Theory", IEEE Trans. Ant. Prop., AP-16, No. 4, (1968).

8. Longuet-Higgins, M., "Reflection and Refraction at a Random Moving Surface. Parts I - III"Opt. Soc. Am. J., 50, pp. 838-856, (1960).

9. Barrick, D. E., "A Review of Scattering From Surfaces with Different Roughness Scales", Radio Science, 3 (New Series), (1968).

10. Barrick, D. E., "Radar Clutter in an Air Defense System Part I. Clutter Physics", Battelle Memorial Institute, Columbus Laboratories, Columbus, Ohio, Contract No. DAAH01-67-C-1921, (January 26, 1968).

11. Ruck, G., D. Barrick, and W. Stuart, Radar Cross Section Handbook, Chapter 9. New York: Plenum Press, (1968).

12. Valenzuela, G. R., "Depolarization of EM Waves by Slightly Rough Surfaces", IEEE Trans. Ant. Prop., AP-15, pp. 552-557, (1967).

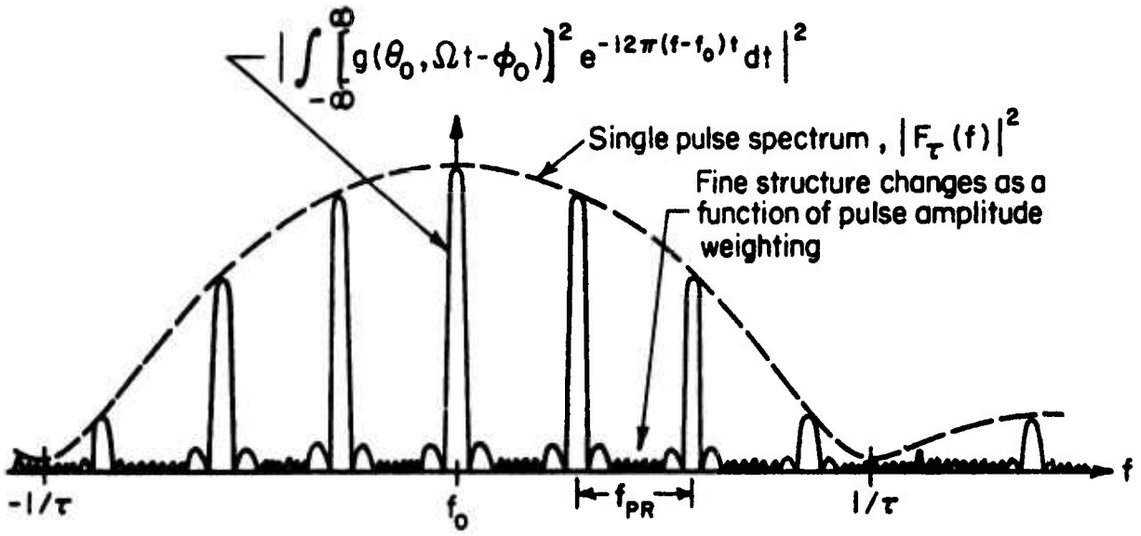

FIGURE 1. SPECTRUM OF PULSE TRAIN MODULATED BY ROTATING ANTENNA PATTERN.

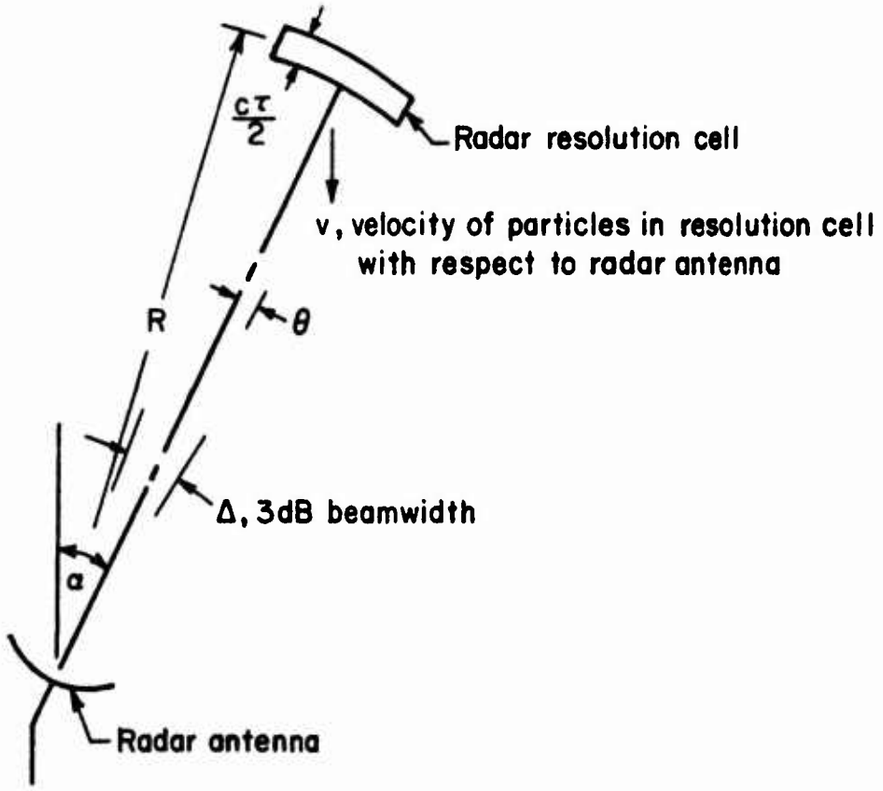

a. Volume - Distributed Scatterers in Resolution Cell

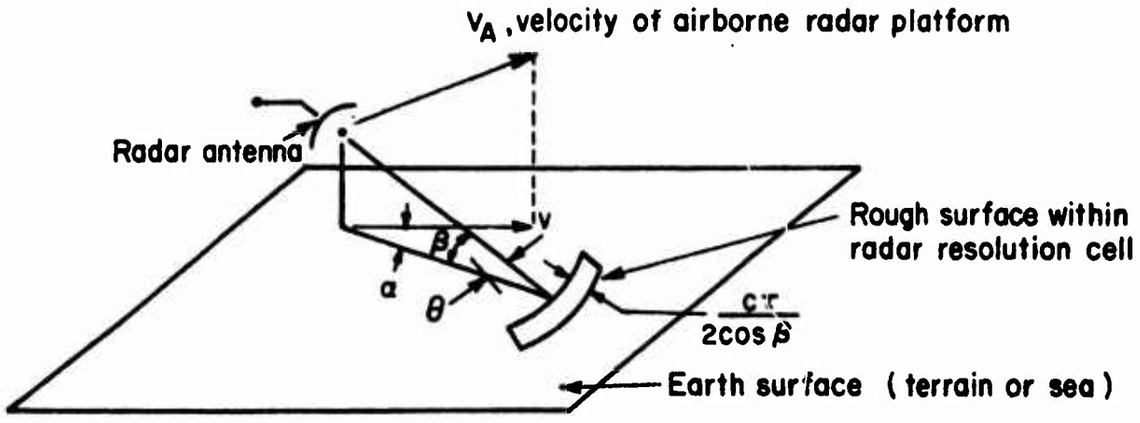

b. Surface within Radar Resolution Cell

FIGURE 2. GEOMETRY OF RADAR AND DISTRIBUTED SCATTERERS FOR FINITE BEAMWIDTH.

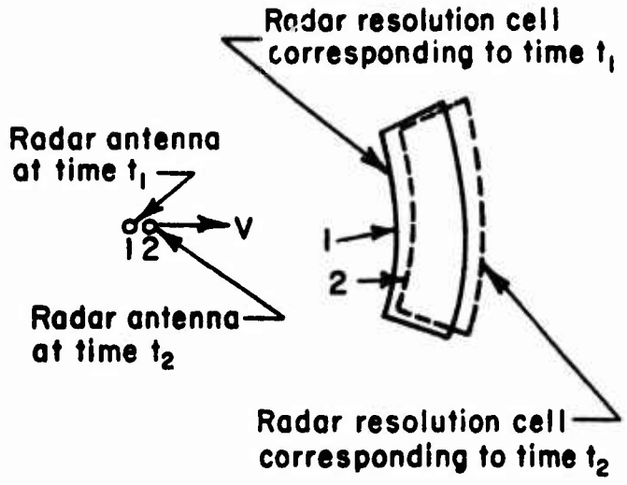

FIGURE 3. GEOMETRY OF DISTRIBUTED SCATTERERS AT GIVEN RANGE FROM MOVING ANTENNA AS VIEWED AT TWO DIFFERENT TIMES.

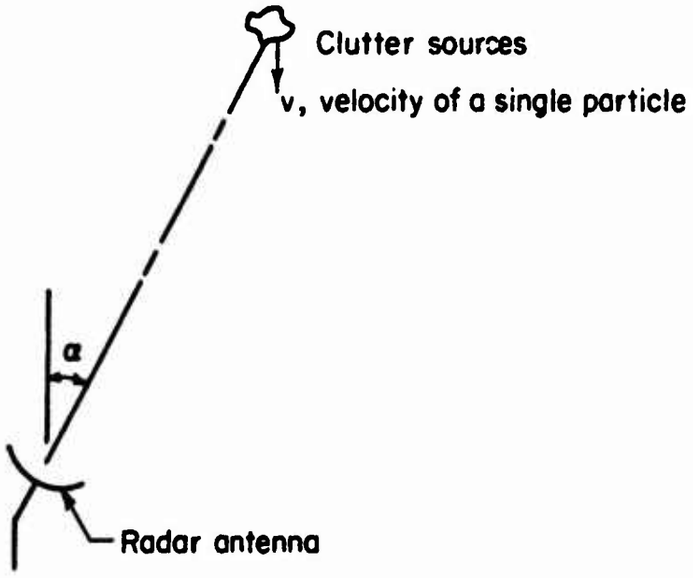

FIGURE 4. GEOMETRY OF VOLUME-DISTRIBUTED SCATTERERS MOVING AT VELOCITIES CLOSE TO v WITH RESPECT TO ANTENNA.